NRIAG JOURNAL OF ASTRONOMY AND GEOPHYSICS
2020, VOL. 9, NO. 1, 226–237
https://doi.org/10.1080/20909977.2020.1728866

Study of nonlinear time series and wavelet power spectrum analysis using solar wind parameters and geomagnetic indices

E. O Falayi[a], A. T. Adewole[b], A. D. Adelaja[a], O. O. Ogundile[a] and T. O. Roy-Layinde[c]

[a]Department of Physics, Tai Solarin University of Education, Ijagun, Ijebu-Ode, Nigeria; [b]Federal College of Forestry, P.M.B. 5087, Jericho, Ibadan. Oyo State. Nigeria; [c]Department of Physics Olabisi Onabanjo University, Ago-Iwoye, Nigeria

ABSTRACT

We investigate the time series of solar wind parameters (interplanetary magnetic field, Bz and solar wind speed, Vx) and geomagnetic indices (disturbance storm time, Dst and auroral electrojet, AE) using wavelet analysis and nonlinear dynamics time series techniques. The data were collected from the Flight Center Space Physics Data Facility (GSFC/SPDF) OMNIWEB interface between 2008 and 2017. Wavelet power spectrum (WPS) analysis assists in breaking down the time series of Bz, Vx, Dst and AE parameters into different scales. It was noted that there is a greater concentration of power between the 512 and 1024 months bands across the Bz, Vx, Dst and AE parameters. We also applied non-linear time series modelling methods to examine the Bz, Vx, Dst and AE parameters. We utilised both the time delay and embedded dimension in computing average mutual information (AMI) and false nearest neighbors (FNN), respectively. The Lyapunov exponent (LE) is used to express the complexity of the nonlinear dynamics based on embedding parameters. The Lyapunov exponents depict positive values which confirm that the complex solar wind parameters and the geomagnetic indices are deterministic chaotic systems. The results show noticeable chaotic characteristics in the Bz, Vx, Dst and AE parameters.

ARTICLE HISTORY
Received 30 September 2019
Revised 18 January 2020
Accepted 1 February 2020

KEYWORDS
Chaos; nonlinear dynamics; solar wind parameters; geomagnetic indices; wavelet power spectrum

1. Introduction

Interplanetary medium variations are caused by solar wind parameters such as variation in flow speed, flow pressure, density, temperature and interplanetary magnetic field (IMF). These variations create geomagnetic disturbances in the magnetospheric and ionospheric current systems. The expulsion of energetic-charged particles intersecting with the Earth's trajectory can have a serious influence on the Earth's magnetosphere. The magnetospheric activity is triggered by the interaction between the geomagnetic field and the solar wind, which results into geomagnetic storms, turbulence, ionospheric currents, auroras, and magnetic reconnection, which are quantified by the global magnetospheric indices. The geomagnetic indices, AE (auroral electrojet), Dst (disturbance storm time), Kp and Ap (planetary indices) depict the intensity of the storm time geomagnetic perturbation of the Earth magnetosphere.

In this research, numerical tools such as chaos techniques and wavelet transformation are employed to understand the dynamics of natural time series. The chaos theory offers the most recent way to describe the unknown facts in random-like data. Chaotic techniques are used to recognise deterministic components, which are varied with other stochastic components in the data. Numerous fields are making use of chaos (nonlinear) techniques because of applicable mathematical models are readily accessible for quantifying and demonstrating nonlinear fluctuations in time-series data, for example, climate and weather forecast (Sharma and Veeramani 2011; Jani et al. 2014; Fuwape et al. 2016; Suresh and Selvaraj 2017), prediction of sunspot (Ossendrijver 2003; Rüdiger and Hollerbach 2004; Zivkovic and Rypdal 2011; Gkana and Zachilas 2015; Sarp et al. 2018), astronomy (Hanslmeier and Brajša, 2010), hydrology (Sivakumar 2000, 2004; Elshorbagy et al. 2002; Yang et al., 2011). The idea of chaos is applied to ionospheric and magnetospheric studies during the quiet and turbulence situation using time series analysis (Chen and Sharma 2006; Rabiu et al. 2014; Ogunsua et al. 2014; Oludehinwa et al. 2014). Unnikrishnan and Ravindran (2010) used chaos techniques to examine the study chaoticity of equatorial and low latitude ionosphere over the Indian subcontinent during geomagnetically quiet and disturbed periods. Unnikrishnan (2010) investigated the GPS TEC variation over the mid-latitude region of Japan and equatorial/low latitude regions of India using nonlinear time series.

Also, wavelet power spectrum (WPS) have been widely used in numerous-related fields (Beltrán and Ponce de León 2010; Hafez et al. 2010; Mandrikova et al. 2010, 2011, 2012a, 2012b, 2012c, 2013; Hafez and Ghamry 2011; Liming et al. 2011; Ghamry et al. 2012; Gwal et al. 2012; Bakhshi et al. 2013; Castillo et al. 2013; Han and Chang 2013). WPS present facts on the

CONTACT E. O Falayi olukayodefalayi@yahoo.com Department of Physics, Tai Solarin University of Education, Ijagun, Ijebu Ode, Nigeria

amplitude of phase signals during the time series and how its amplitude changes with time. WPS is used to investigate irregular time series and to reveal the short occurrence inside the time series. Wavelet transformations determine complex analysis by breaking down and changing from a dimensional time series into two-dimensional time-frequencies domain. Torrence and Compo (1998) recognised that wavelet transforms allow recognition of the major periodicities in a time series and it is used to examine the development of each frequency. At a particular frequency, the wavelet spectrum offers qualitative facts about the power present in each time series. Falayi et al. (2017) used the wavelet power spectrum to investigate the geomagnetic storm of 17 March and 22 June 2015 during the solar cycle 24 over the selected station at Addis Ababa, Mbour, Hermanus, Hartebeesthoek and Tamanrasset the equatorial and mid-latitudes of Africa. Also, the geoelectric field of the horizontal variation was studied during 2003 events at Abisko, Nurmijarvi, Sodanklya, and Uppsala using wavelet power spectrum (Falayi et al. 2018). It was noted that high-latitude stations exhibit high geoelectric field variations for the period of the disturbance caused by a coronal mass ejection.

In this research, we examine solar wind components (solar wind, Vx, and interplanetary magnetic field, Bz) and geomagnetic indices (Disturbance storm time, Dst and auroral electrojet, AE) from 2008 to 2017 using nonlinear time series and wavelet power spectrum techniques. This paper is structured as follows. Section 2 describes the observational data used in this study. Besides, this section examines the wavelet power spectrum analysis and nonlinear dynamics time series of the Bz, Vx, Dst and AE. In Section 3, the wavelet spectrum approach and the time-dependent dynamical complexity of the coupled solar wind-magnetosphere system for the Bz, Vx, Dst and AE are discussed. Section 4 summarises the findings with the concluding remarks.

2. Data and methods

Here, we analyse the solar wind parameters (solar wind speed, Vx and interplanetary magnetic field IMF, Bz) and geomagnetic indices (disturbance storm time, Dst and auroral electrojet, AE). The 1-hour resolution data used were obtained from the Flight Center Space Physics Data Facility (GSFC/SPDF) OmniWeb (http://omniweb.gsfc.nasa.gov) interface between 2008 and 2017. The AE index shows the activity of the electrojet in the auroral region (Davis and Sugiura 1966). The AE index reveals the irregularities connected with magnetospheric dynamics as a result of solar wind variation. Consequently, AE index is known to correspond to the dynamics of the magnetospheric system (Hajkowicz 1998). The Dst measures the intensification of the ring current and it is widely applicable in different research areas on the solar wind-magnetosphere coupling particularly during geomagnetic storms (Mayaud 1980). The Vx shows the strong point of the geomagnetic disturbance. The Bz is the interplanetary magnetic field which tends southward as an indication of the geomagnetic storms.

2.1. Wavelet power spectrum analysis (WPS)

The main benefit of the WPS investigation technique is to give facts about the frequency of the occurrence in relation to its locality in the time series. The WPS is produced by enlargement, $\Psi(t) \rightarrow \Psi(t)$, and translations $\Psi(t) \rightarrow \Psi(t+1)$ with respect to time t. The mother wavelet is expressed in Equation (1) as:

$$\Psi_{a,b}(t) = a^{\frac{1}{2}}\psi\left(\frac{t-b}{a}\right), \tag{1}$$

where a correspond to the scale related to increase and reduction from the wavelet and b symbolise the time localisation. Equation (2) is expressed as Morlet wavelet (Torrence and Compo 1998):

$$\Psi(t) = \frac{e^{iw_o t}}{\sqrt[4]{\pi}e^{\frac{t^2}{2}}}, \tag{2}$$

where w_o is the dimensionless frequency. The use WPS on $x(t)$ time series is referred to as the convolution of the data series of the Morlet wavelets in Equation (3) (Kumar and Foufoula-Georgiou 1997; Torrence and Compo 1998):

$$WPS(a,b) = \int_{-\infty}^{\infty} x(t)\Psi^*{}_{a,b}(t)dt, \tag{3}$$

where $\Psi^*{}_{a,b}(t)$denotes as the conjugate of wavelet function $\Psi_{a,b}(t)$. The expression of the wavelet coefficient at time index n and scale a is expressed in Equation (4):

$$WPS_n(a) = \sum_{n^l=0}^{N-1} x(n^l)\psi * \left[\frac{(n^l-n)dt}{a}\right], \tag{4}$$

where N is the length of the data time series and dt represents the time interval. The scale-averaged WPS is used to examine variation in power over a band of scales given in Equaation (5) (Torrence and Compo 1998):

$$\overline{W_n^2} = \frac{\partial j \partial t}{0.776}\sum_{j=j1}^{j2}\frac{|W(a_j)|^2}{a_j}. \tag{5}$$

The global wavelet spectrum (GWS) is employed to recognise the most energetic phase present on the cross-wavelet analysis. The GWS is expressed in Equation (6):

$$GWS = \int |WPS(a,b)|^2 db. \quad (6)$$

Figures 1(a–d)–4(a–d) depict the wavelet power spectrum analysis to estimate the time-frequency characteristic of the solar wind parameters (Bz, Vx) and geomagnetic indices (Dst, Kp and AE) variation between 2008 and 2017.

2.2. Time series analysis

2.2.1. Detrend of data analysis

A statistical technique of eliminating trend from the time series data is referred to as detrending. Detrending is regularly used to eliminate a characteristic thought to alter the relationships of concerned parameters. In this research, since our attention is to study complexities in a rapidly fluctuating data set, it is necessary to eliminate long term or seasonal trends, so that we can analyse the basic variations in the recorded time series data (see Figure 5). It is also used as a preprocessing stair to arrange time series for analysis of techniques that assume stationarity. In this section, certain detrending procedures are applied as the only preprocessing stairs. In this approach, a straightforward additive superposition of trend and variability time series can be break down as: $y(t) = T(t) + r(t)$, where $r(t)$ represents residual, variability around the trend $T(t)$. The variation components can posses both the stochastic and deterministic components.

2.2.2. Techniques of nonlinear dynamics time series

To investigate the chaotic time series of Bz, Vx, Dst and AE indices, we evaluate the average mutual information (AMI), false nearest neighbour (FNN), Lyapunov exponent and phase space construction. We seek to obtain a suitable embedding dimension (m) that is required to reconstruct phase space. The structure can be described by the embedding dimension. Phase spaces reconstructions are derived from the changes in the coordinates and it explains the time progression. The techniques of delays are applied to

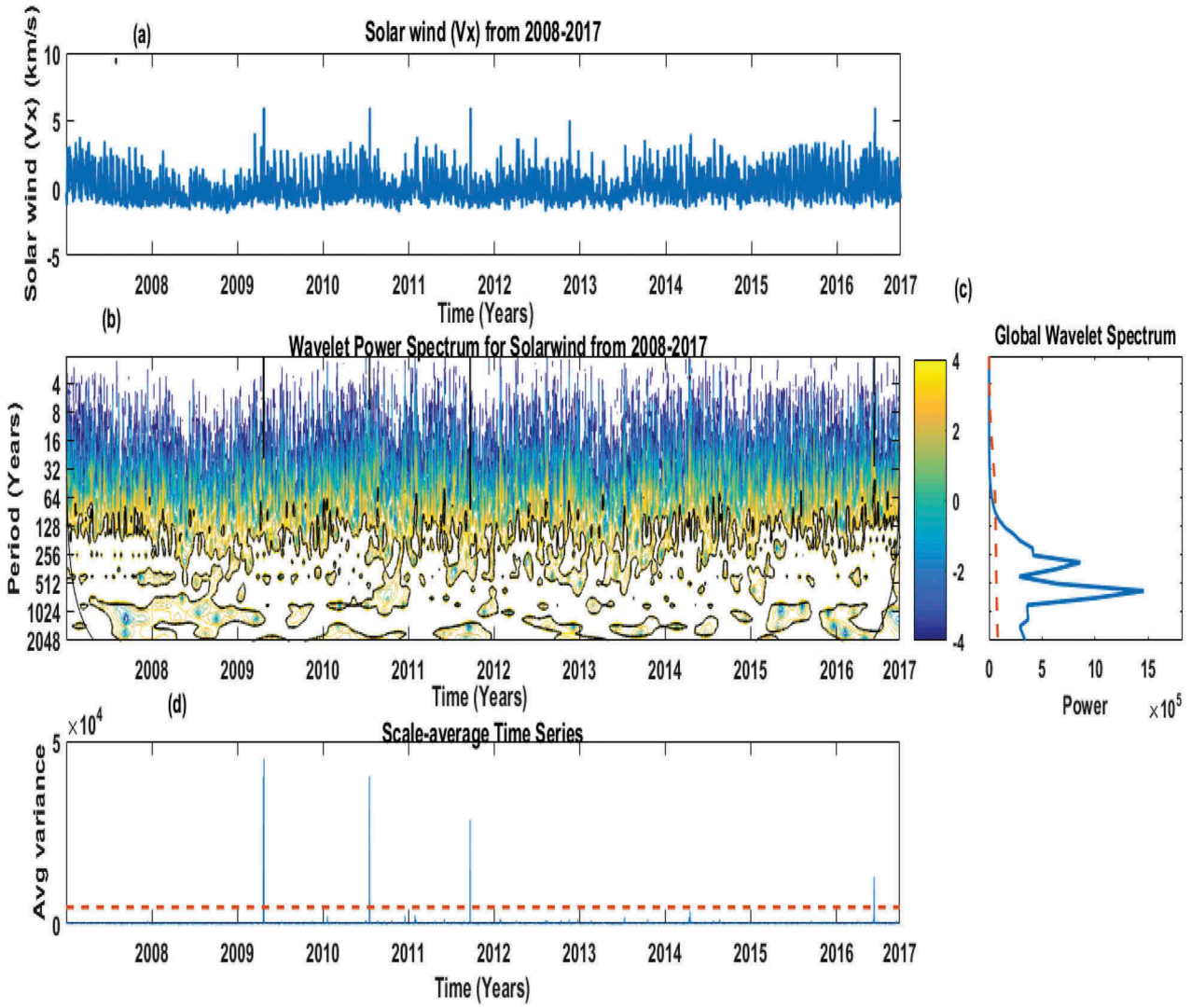

Figure 1. (a) Vx data from Ominiweb observatory for 2008–2017. (b) Wavelet power spectrum of Vx index between 2008 and 2017, with concentration of power between 512 and 1024 months. (c) GWS, while the breaking lines symbolise significance level of 5% (d). The broken lines in scale-average time series symbolise confidence level of 95% for Vx.

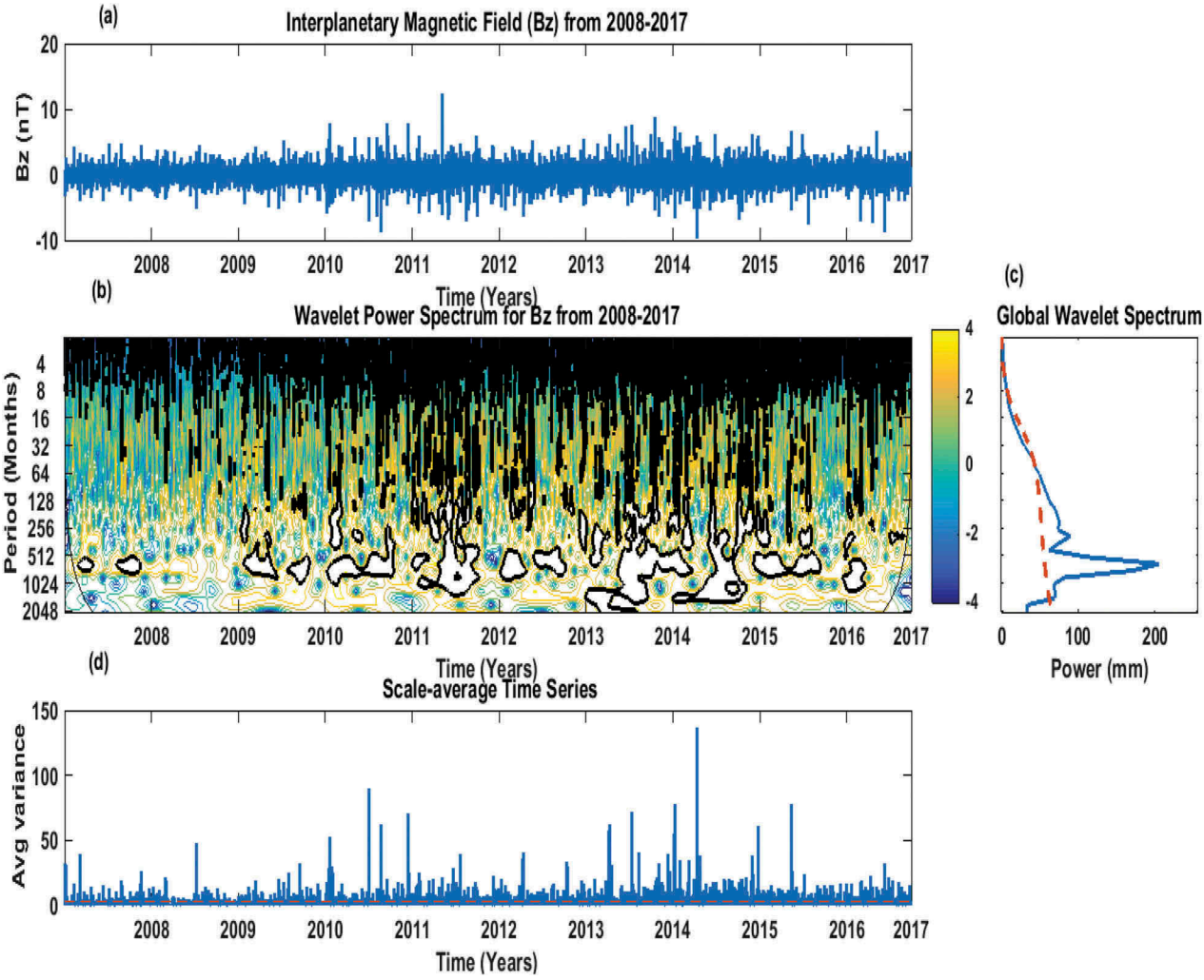

Figure 2. (a) Bz index data from Ominiweb observatory for 2008–2017. (b) Wavelet power spectrum of Bz index between 2008 and 2017, with concentration of power between 512 and 1024 months. (c) GWS, while the breaking lines symbolize significance level of 5% (d). The broken lines in scale-average time series symbolize confidence level of 95% for Bz index.

reconstruct phase space and this can be the most significant in phase space reconstruction system. The phase space reconstruction assists to make known the multidirectional feature of the structure and rely on the embedding theorem. The phase space is reconstructed to demonstrate the multidimensional structure which is expressed in Equation (7):

$$T(n) = \{X_n, X_{n+\tau}, X_{n+2\tau}, \cdots, X_{n(m-1)\tau}\}, \qquad (7)$$

where T_n correspond to as the vector in phase space, the symbol m is described as the embedding dimension and τrepresent to as the delay time.

2.2.3. Average mutual information (AMI) technique

The average mutual information is computed from Bz, Vx, Dst and AE indices. The phase space construction can be obtained from the initial minimum of AMI (Shaw 1981), the initial minimum of the AMI is chosen as delay time. The appropriate measure for determining τ is the AMI between x_n and $x_{(n+\tau)}$ (Fraser and Swinney 1986). From the time series {$x0$, $x1$, $x2$, …, xi, …, xn}, the minimum ($x_{\min}$) and the maximum ($x_{\max}$) of the series can be used to obtain the absolute difference $|x_{\max} - x_{\min}|$ values. However, the difference is partitioned into j equally sized period, where $\boldsymbol{j}$ is a huge integer number expressed in Equation (8):

$$M(\tau) = -\sum_{q=1}^{j}\sum_{r=1}^{j} p_{qr}(\tau)\ln\frac{p_{qr}(\tau)}{p_q p_r}. \qquad (8)$$

The symbols P_q and P_r are the probabilities that the variable assume a value in the qth and rth bins, respectively. While $P_{q,r}(\tau)$ represents the combined probability that x_n is in bin $\boldsymbol{q}$ and $x_{(n+\tau)}$is in bin $\boldsymbol{r}$.

2.2.4. False nearest neighbour (FNN) evaluation

FNN is an appropriate technique for evaluating the optimal embedding dimension for Bz, Vx, Dst and AE indices. For this reason, the algorithm gets rid of the incorrect neighbours (Kennel et al. 1992). The major concept is to investigate how the number of FNN changes along the trajectory with increase in embedding dimension. In one dimension, the points are near to one another as a result of projection, this will be segregated in upper

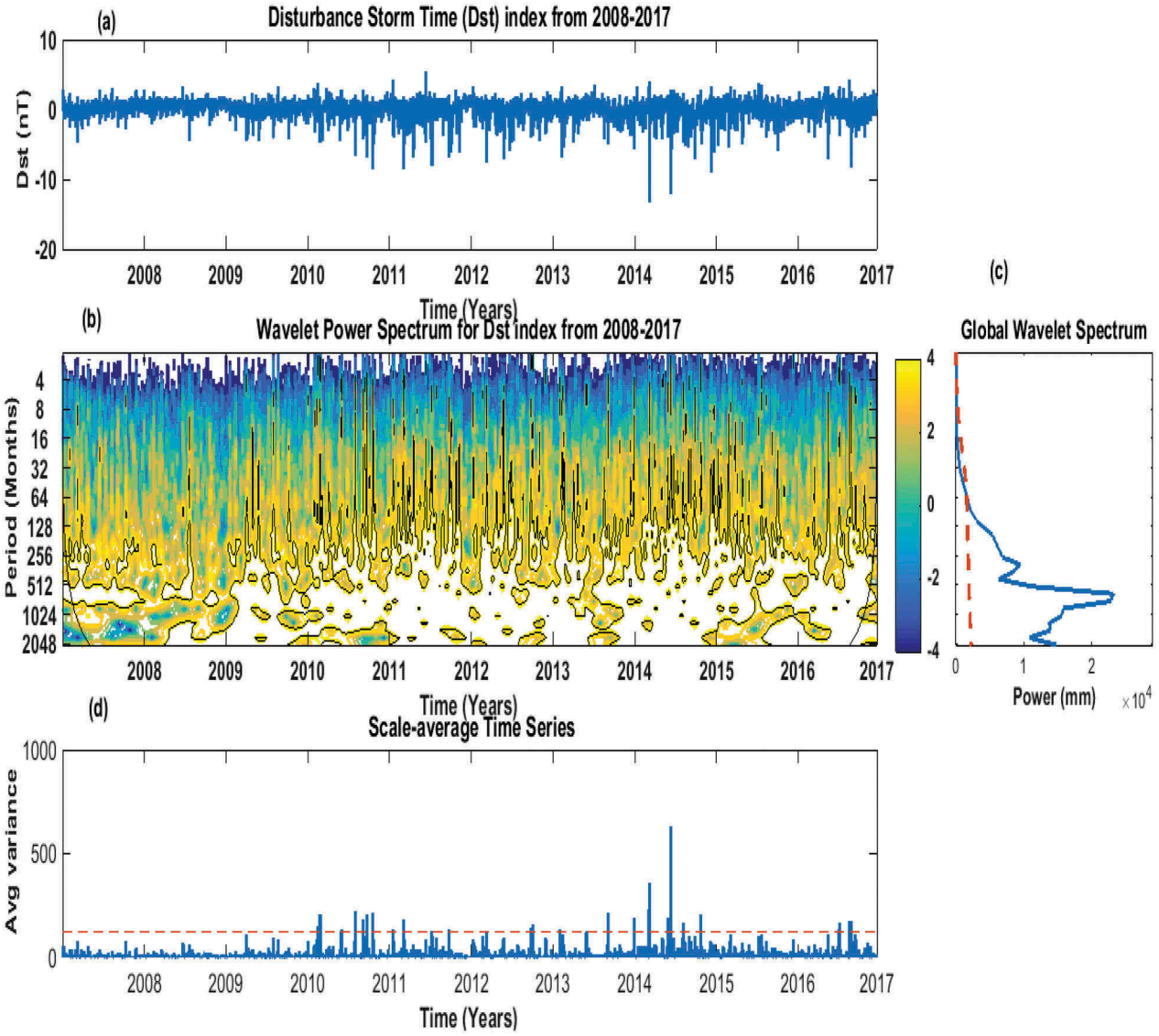

Figure 3. (a) Dst index data from Ominiweb observatory for 2008–2017. (b) Wavelet power spectrum of Dst index between 2008 and 2017, with concentration of power between 512 and 1024 months. (c) GWS, while the breaking lines symbolize significance level of 5% (d). The broken lines in scale-average time series symbolize confidence level of 95% for Dst index.

dimensions. The difference between two relative distance neighbour points intensify, when moving from d to $d+1$ and it is a measure for casting embedding errors (Abarbanel et al. 1990; Suresh and Selvaraj 2017). This measure is referred to as false nearest neighbour distance, which is expressed in Equation (9) as:

$$\left[\frac{R^2{}_{d+1}(n,r) - R^2{}_d(n,r)}{R^2{}_d(n,r)}\right]^{\frac{1}{2}} = \frac{|x(n+\tau) - x(t_r+\tau)|}{R_d(t,r)} > R_{tot}, \tag{9}$$

where t and t_r represents corresponding times to neighbour and original points, respectively, R_d is called the distance in the phase space with embedding dimension d. While R_{tot} is the threshold tolerance. The FNN plots are employed in this study using Equation (9) (see Figure 7(a–d)).

2.2.5. Lyapunov exponents (LE)

The LE is used to explain when the near trajectories diverge or converge. The trajectories converge and the structure are stable when the exponents are zero or negative. The trajectories diverge and the structure remains unstable if the Lyapunov exponent is positive, that is the structure remains chaotic (Eckman and Ruelle 1985). A huge LE is significant, due to high limit of exactness for any predictive model that is not always restructured. The average exponential rate of divergence of two originally near paths was explained using Equation (10):

$$\lambda = \lim \frac{1}{n} \ln \frac{|\Delta x(x_o, n)|}{|\Delta x_o|}, \tag{10}$$

where λ represent Lyapunov exponents (LE) and it is applied for differentiating different kinds of paths and to determine the rate of divergence (Shaw 1981; Bahr

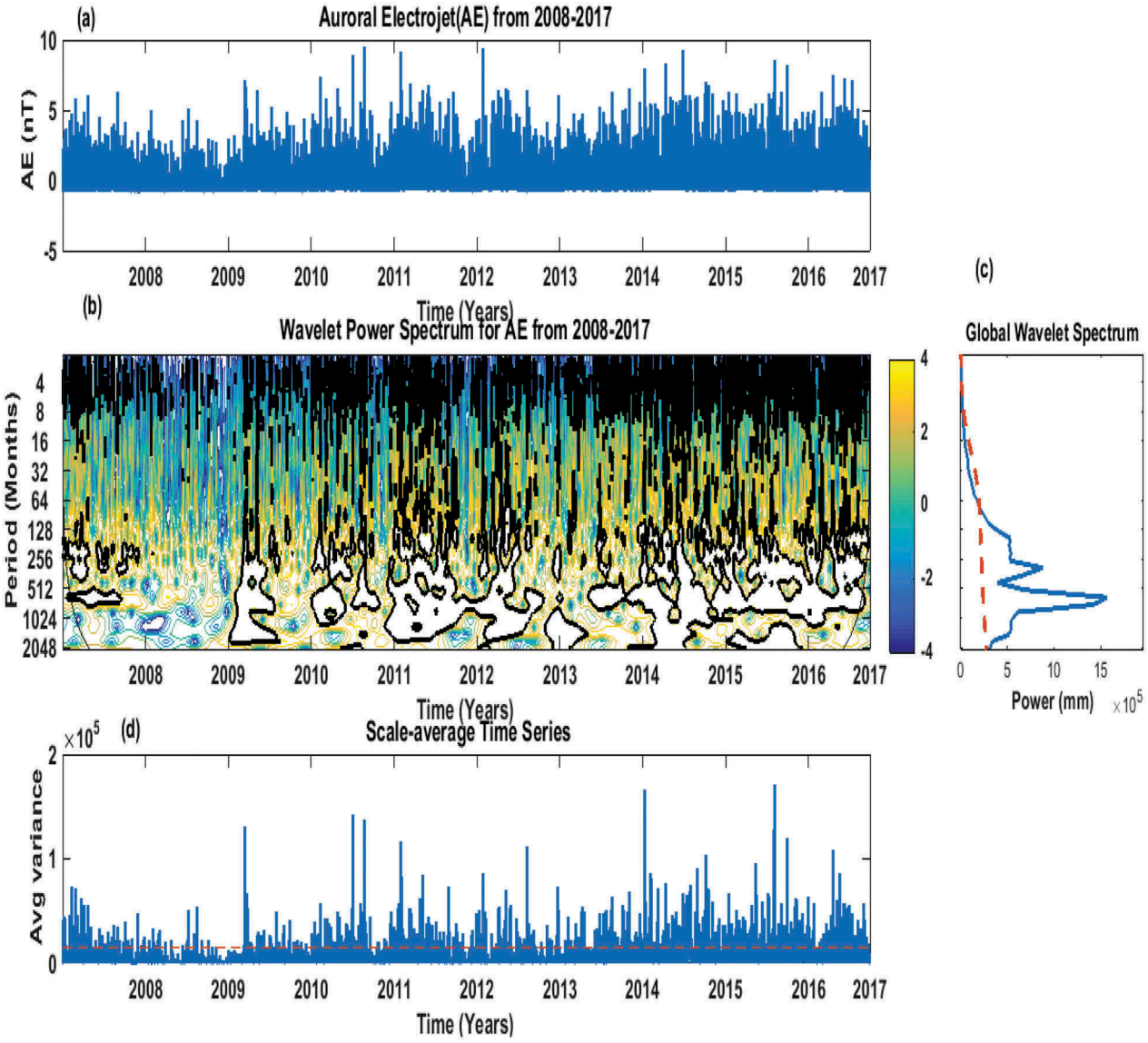

Figure 4. (a) AE index data from Ominiweb observatory for 2008–2017. (b) Wavelet power spectrum of AE index between 2008 and 2017, with concentration of power between 512 and 1024 months. (c) GWS, while the breaking lines symbolize significance level of 5% (d). The broken lines in scale-average time series symbolize confidence level of 95% for AE index.

and Froyland 1992). The exact estimation of a chaotic dynamical structure is a component of the major Lyapunov exponent (Abarbanel and Lali 1996) which is expressed in Equation (11):

$$\Delta n = \frac{1}{\lambda_{\max}}. \tag{11}$$

The Lyapunov exponent plots of Bz, Vx, Dst and AE indices are obtained using Equations (10) and (11) is presented in Figure 8(a–d).

2.2.6. Phase space reconstruction

Figure 9(a–d) illustrates the phase space reconstruction path for the Bz, Vx, Dst, AE time-series parameters. It was noted that changes in the phase space pattern were observed with different variables from the present study.

3. Discussion of the results

The wavelet power spectrum was used to decompose the solar wind, interplanetary magnetic field, disturbance storm time and auroral electrojet time series into different scales. The WPS examines the non-stationary signal which allows the classification of solar wind, interplanetary magnetic field, auroral electrojet and disturbance storm in time series. The results provide us with more information about the progression of these irregularities in frequency and time mode.

Figures 1(a)–4(a) show typical time series from the raw data of the solar wind, interplanetary magnetic field, disturbance storm time and auroral electrojet parameters from 2008 to 2017. On the other hand, Figures 1(b)–4(b) illustrates the power of the WPS for the solar wind, interplanetary magnetic field, disturbance storm time and auroral electrojet parameters.

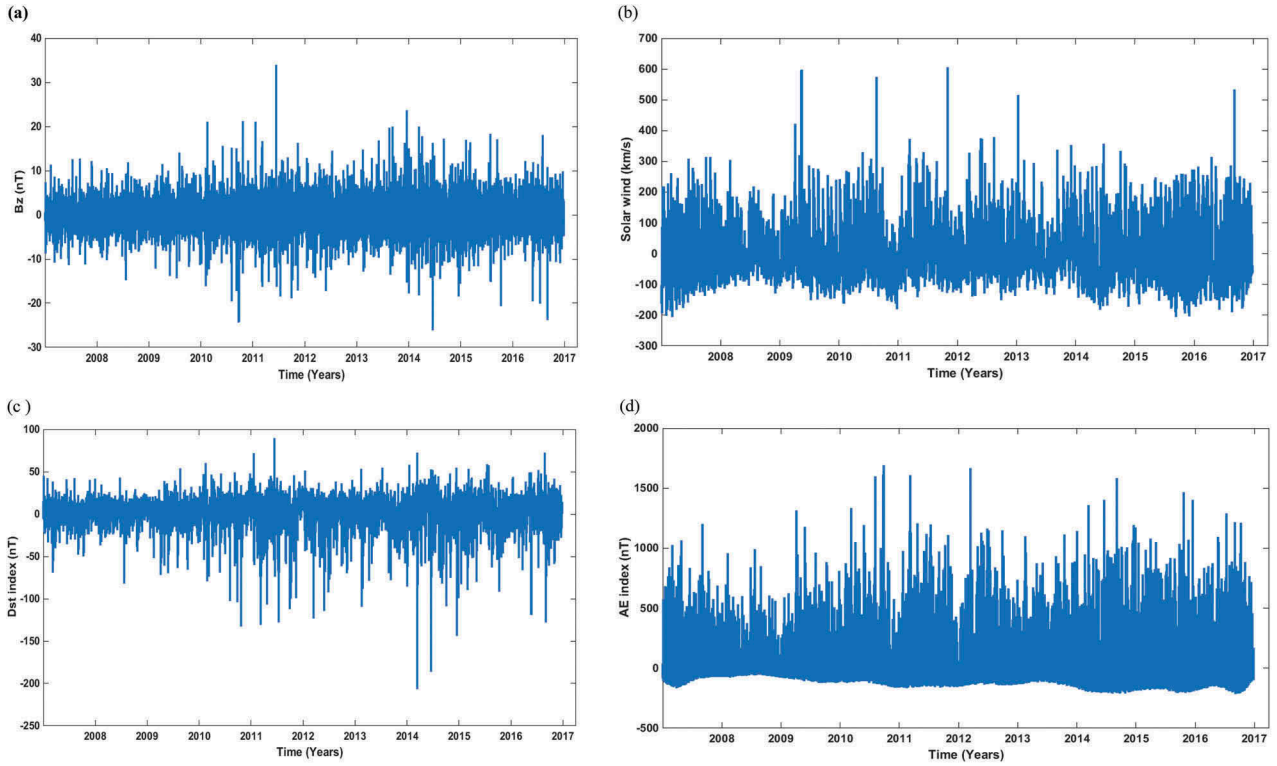

Figure 5. The detrended time series data for (a) Bz, (b) Vx, (c) Dst index, (d) AE index data obtained from Ominiweb from 2008 to 2017.

Figures 1(b)–4(b) show the real fluctuation of the wavelets character relative to their magnitude. The highest energy of the signal over the period is represented by the colour red while weaker intensity represents blue colour. The energy distribution of WPS is concentrated between the periodic cycles of 512–1024 months band with maximum variability. This implies that the time series is a powerful annual indicator for solar wind, interplanetary magnetic field, disturbance storm time and auroral electrojet parameters (see Figures 1(b)–4(b)). The weak variation implies reductions of the power within the band periodic cycles. The blank space denotes the missing data gaps. The global wavelet spectrum (GWS) of Figures 1(b)–4(c) examines the prevailing periods of the signals of solar wind, interplanetary magnetic field, disturbance storm time and auroral electrojet data for different periods. Figures 1(b)–4(c) illustrate the significant peaks above the 95% confidence level for the GWS, which are represented by the dashed lines. The assessment of the parameters is the confidence level. The usual variable is the 95% confidence level and is corresponding to 5% level of significance. The various peaks in the global spectra signify that the signal is made of fluctuations with different time phase and with different amplitude. The amplitude of the GWS specifies the obtainable potential for the analysed signal. The distribution of feature scales basically controls the global wavelet spectrum shape (see Figures 1(b)–4(c)). Figures 1(b)–4(d) exhibit the scale-average wavelet power and is a time series of the mean variation in a definite band. We noticed that 512–1024 months can be used to investigate the modulation of both frequency and time series. The figures are composed by the mean of Figures 1(b)–4(b) across the scales between 512 and 1024 months, this produces a measure of the yearly mean variation against time. This approach was engaged to validate the wavelet results and to obtain the periodicity content of the Vx, Bz, Dst, and AE time series. The similar results attained between 512 and 1024 months reveal different periodicities tend to appear with no stable structure during each year. The significant amplitude of WPS was seen in all the years. It can be noticed that Vx, Bz, Dst and AE are affected at the time of geomagnetic storm. This occurrence could possibly be attributed to the dominance of coronal mass ejections during high solar activity geomagnetic storms. On the contrary, when the solar activity is low the wavelet coefficients exhibit low power spectrum energy. Richardson et al. (2002) established that geomagnetic storms are connected by streams of high solar wind speed emanating from coronal holes and are frequent during the decline phase of the solar cycle which are usually small in amplitude in contrast to solar maximum conditions.

The AMI and FNN techniques provide an understanding of the complexity of the fundamental system. Figure 6(a–d) shows the AMI in bits with time delay function of Vx, Bz, Dst, and AE time series between

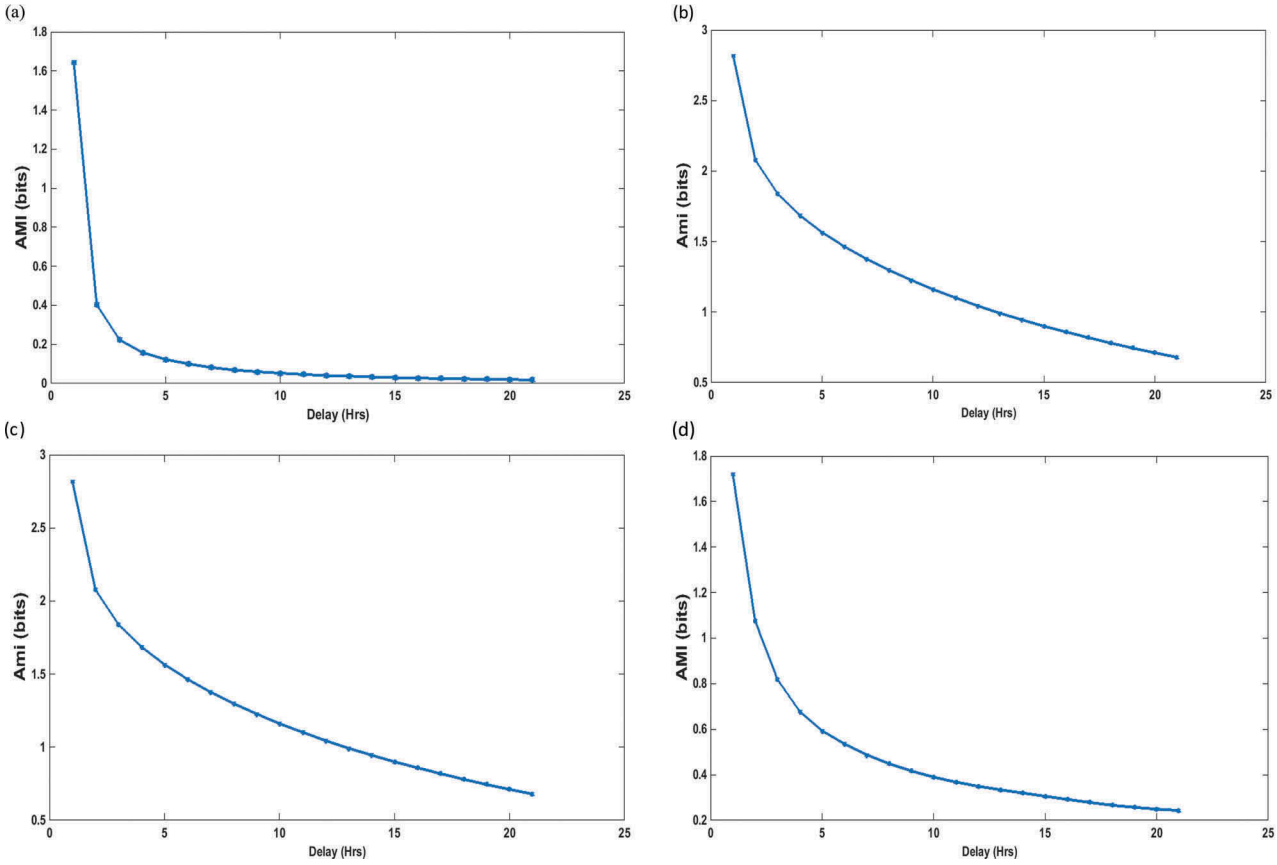

Figure 6. (a–d): Average mutual information in bits against the delay time in hours obtained from detrended time series for (a) Bz, (b) Vx, (c) Dst index, (d) AE index data obtained from Ominiweb from 2008 to 2017.

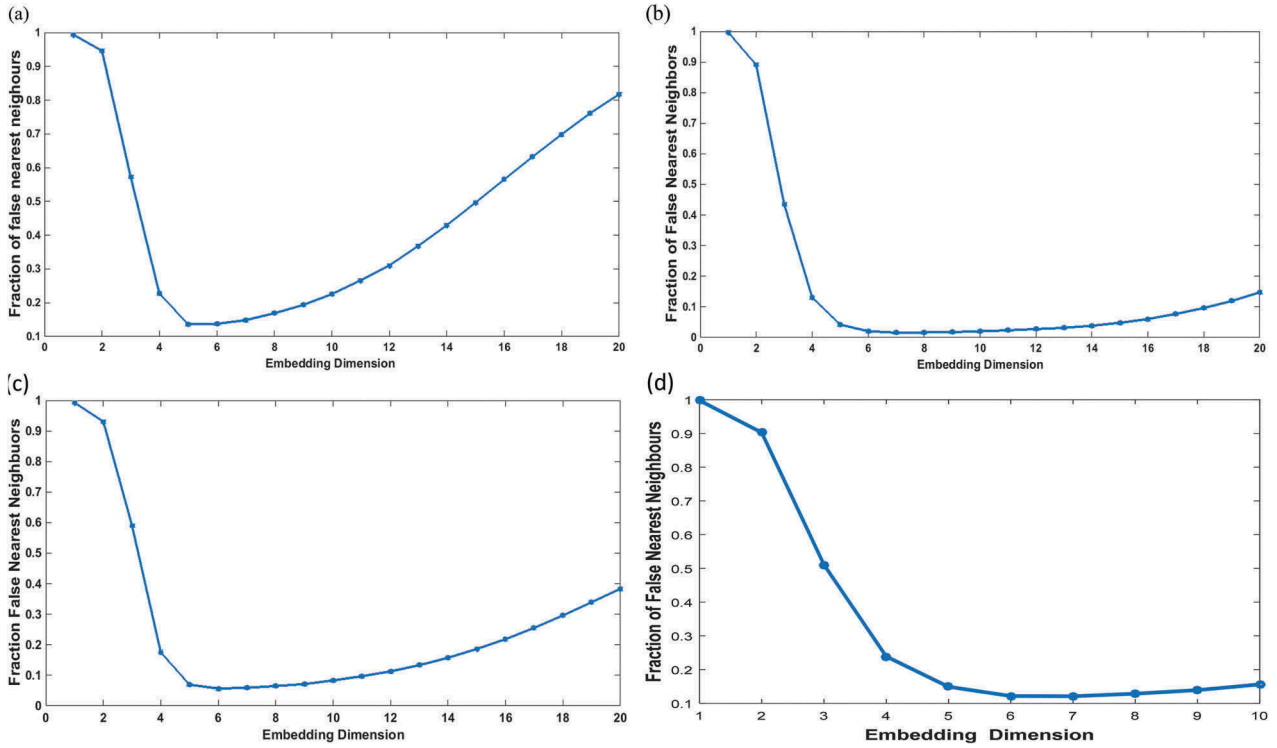

Figure 7. (a–d): Fraction of false nearest neighbour Vs embedding dimension obtained from detrended time series for (a) Bz, (b) Vx, (c) Dst index, (d) AE index data obtained from Ominiweb from 2008 to 2017.

2008 and 2017. We computed AMI in order to derive the time delay function (τ). The embedding dimension was obtained from a geometrical analysis described as false nearest neighbour (see Figure 7(a–d)). When the false nearest neighbours move towards zero, the preferred dimension is attained. For the Vx, Bz, Dst, and

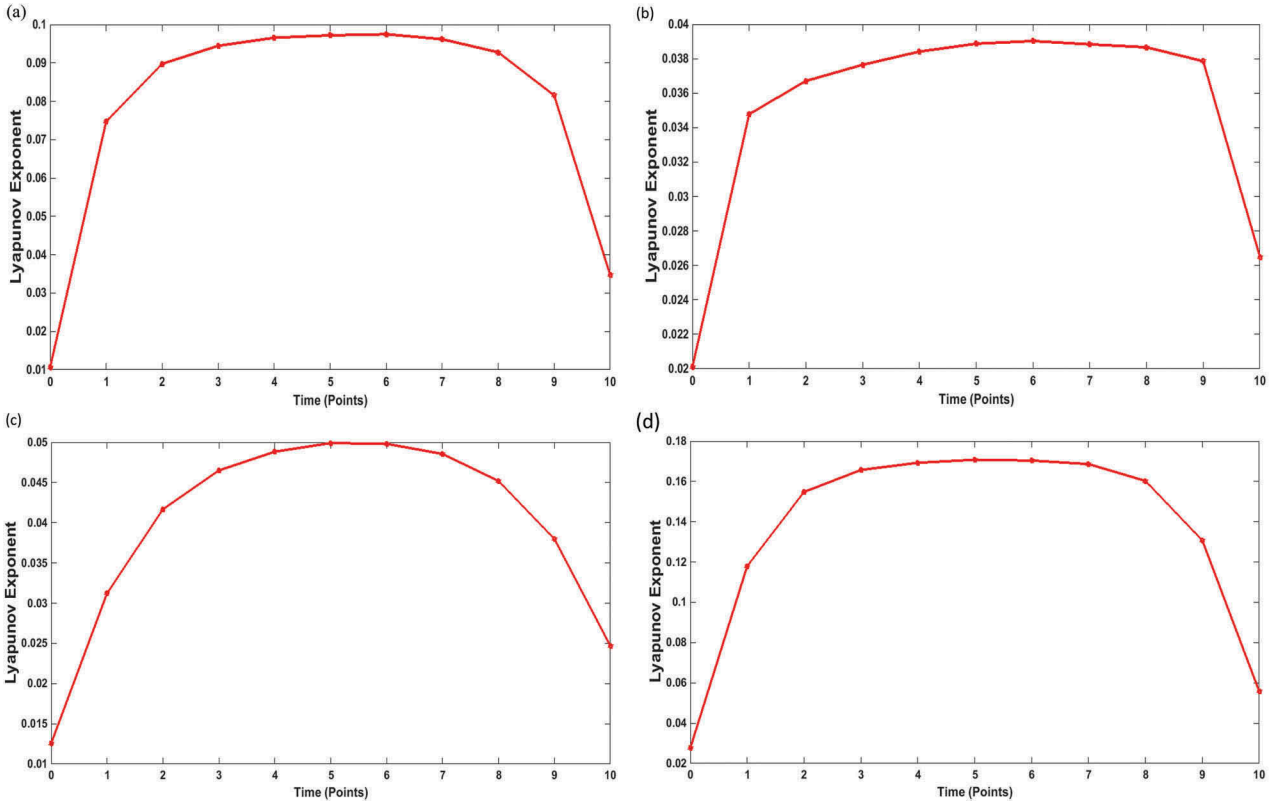

Figure 8. (a–d): Lyapunov exponent obtained from detrended time series for (a) Bz, (b) Vx, (c) Dst index, (d) AE index data obtained from Ominiweb between 2008 and 2017.

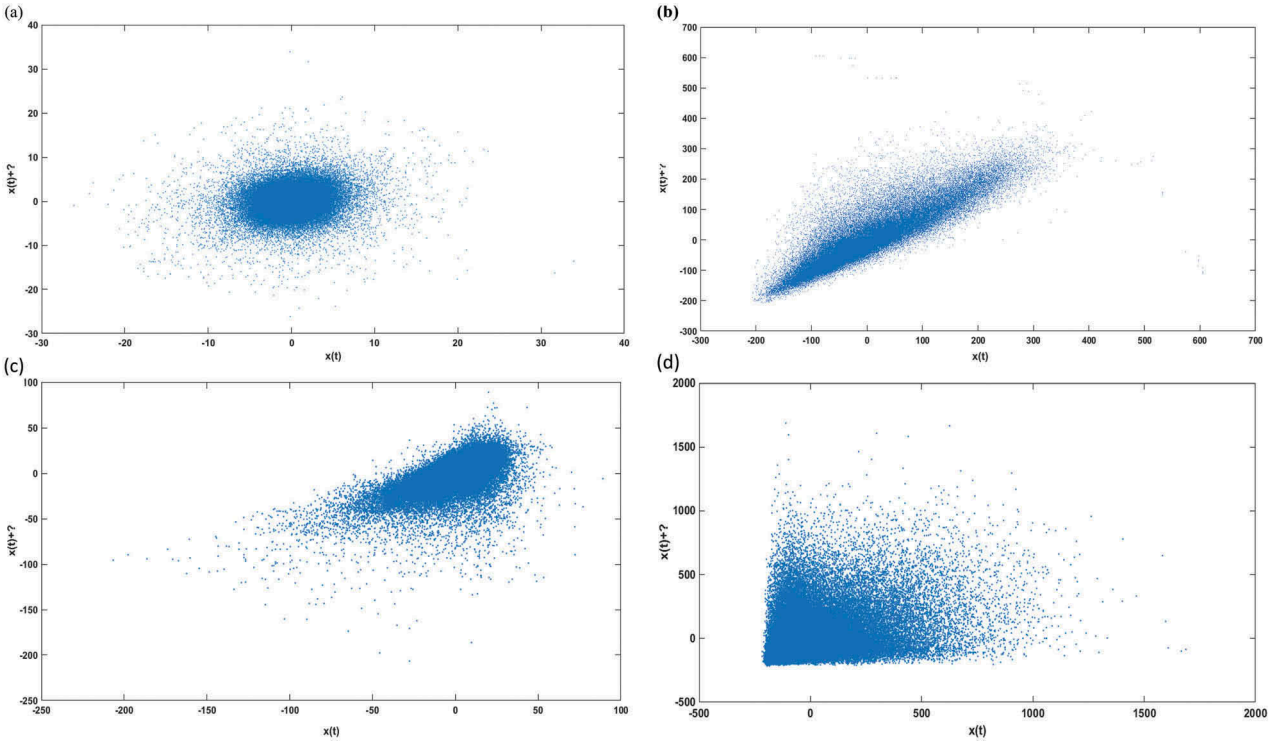

Figure 9. (a–d): Phase space reconstruction obtained from detrended time series for (a) Bz, (b) Vx, (c) Dst index, (d) AE index data obtained from Ominiweb from 2008 to 2017.

AE parameters the minimum Embedding dimension (m) appears to be 5, 7, 6 and 6, respectively (see Figure 7(a–d)). These results describe the residual in any dimension and it provides a quantitative demonstration of how data can be modelled in that dimension. To identify the chaotic behaviour of Bz,

Vx, Dst and AE parameters in a dynamical system, a quantifier – Lyapunov exponent was employed.

Figure 8(a–d) depicts Lyapunov exponent obtained from detrended time series of Bz, Vx, Dst and AE parameters measured from Ominiweb between 2008 and 2017. These results revealed that the positive values of the Lyapunov exponent for Bz, Vx, Dst and AE time series are 0.098, 0.039, 0.05 and 0.17, respectively. This shows a strong indicator for the chaotic behaviour in the parameters (Bhattacharyya 1990). The phase space reconstruction plot of the Bz, Vx, Dst and AE parameters time series is stochastic as illustrated in Figure 9(a–d). It shows that the delay $\tau = 10$ and $5 \leq m \leq 7$ depends on the parameters obtained from AMI and FNN method against the actual time series. It also determines the state of the dynamical system which can be obtained in both identification and predictability using phase space construction.

The result depicts that Sun–Earth is a very dynamical structure in which a constant change of mass, energy and momentum take place between the solar wind and the Earth's magnetosphere during reconnection as suggested by Vasyliunas (1975). The chaotic behaviour of magnetosphere might be the consequence of the joint effect of solar wind and internal magnetospheric activity (Unnikrishnan, 2008). The fluctuation of the magnetosphere-ionosphere system is the reflection of the solar wind fluctuation and has influence on Earth's magnetosphere which structurally extends nonlinearly. The magnetosphere system has internal variability, which can be suppressed and the system might move towards stochasticity preferable than deterministic chaoticity. Solar winds are stochastic drivers which have impact on storm flowing into the system due to CMEs that create the geomagnetic storms. The auroral arcs are weak when the solar wind is not driving the magnetosphere. The strength of the auroral arcs and auroral currents enhances, when the solar wind driving magnetosphere increases, which have impact on Bz, Vx, Dst and AE parameters. Between the period of 2008 and 2017, the nonlinear time series techniques employed using Bz, Vx, Dst and AE parameters and Lyapunov exponent as a quantifier indicates the chaotic behaviour in the magnetospheric dynamic system. The calculation of this Lyapunov exponent from the time series parameters produces positive values of Lyapunov exponent, demonstrating the occurrence of chaos. The Bz, Vx, Dst and AE parameters are able to trace variation connected with the time-dependent dynamical complexity of magnetospheric variability during the storm and quiet periods. The Bz, Vx, Dst and AE parameters exhibit different Lyapunov exponent due to different conditions from coronal mass ejections and magnetic cloud. Lastly, this research investigation indicates that the dynamics in the magnetosphere-ionosphere can be described in detail when high-resolution data and more statistical techniques are used. The evaluation of the persistence feature of the Bz, Vx, Dst and AE parameters connected to the geomagnetic storms can be suggested as a measure for predicting magnetic activity.

4. Conclusion

The study shows the results of the Bz, Vx, Dst and AE parameters using both wavelet spectrum analysis and nonlinear dynamic time series techniques. WPS depicts greater concentration of power between the 512 and 1024 months bands across the Bz, Vx, Dst and AE parameters. This event can be attributed to coronal mass ejections for the period of high solar activity, when the solar activity is low the wavelet coefficients exhibit low power spectrum energy. The results of the nonlinear dynamic time series techniques have revealed that the Bz, Vx, Dst and AE time series is deterministic and can be modelled by means of the phase space method. The phase space methods establish the deterministic nature of the time series, Bz, Vx, Dst and AE which shows a positive value of Lyapunov exponents. The divergence of the trajectories is an indication of chaos which was demonstrated by reconstructing phase space.

Acknowledgements

The authors appreciate the Flight Center Space Physics Data Facility (GSFC/SPDF) OMNIWEB interface (http://www.omniweb. gsfc.nasa.gov) staff for providing solar wind parameters (solar wind speed and interplanetary magnetic field) and geomagnetic indices (Disturbance storm time and auroral electrojet).

Disclosure statement

No potential conflict of interest was reported by the authors.

ORCID

O. O. Ogundile http://orcid.org/0000-0002-2053-6086

References

Abarbanel HDI, Brown R, Kartke JB. 1990. Prediction in chaotic nonlinear systems: methods for time series with broadband Fourier spectra. Phys Rev. 41:1782–1807.

Abarbanel HDI, Lali U. 1996. Nonlinear dynamics of the Great Salt Lake: system identification and perdition. Climate Dyn. 12:287–297.

Bahr U, Froyland J 1992. Introduction to chaos and coherence. Institute of Physics Publishing Ltd. Bristol (Philadelphia and New York). 130 Seiten. 69 Abbildungen + farbige Tafeln. 4 Tabellen. Stichwortverzeichnis. 12.50 (pbk), 29.50 (hbk).

ISBN 0-7503-0195-3 (pbk). ISBN 0-7503-0194-5 (hbk)". In: Crystal Research and Technology 27.8 (1992).
Bakhshi AD, Bashir S, Shah SI, Maud MA. 2013. Non-linear trend estimation of cardiac repolarization using wavelet thresholding for improved T-wave alternans analysis. Digit Signal Process. 23(4):1197–1208.
Beltrán JR, Ponce de León J. 2010. Estimation of the instantaneous amplitude and the instantaneous frequency of audio signals using complex wavelets. Digit Signal Process. 90(12):3093–3109.
Bhattacharyya A. 1990. Chaotic behaviour of ionospheric turbulence from scintillation measurements. J Geophys Res. 17:733–738.
Castillo E, Morales DP, Botella G, García A, Parrilla L, Palma AJ. 2013. Efficient wavelet-based ECG processing for single-lead FHR extraction. Digit Signal Process. 23 (6):1897–1909.
Chen J, Sharma AS. 2006. Modelling and prediction of the magnetospheric dynamics during intense geospace storms. J Geophys Res. 111:A04209.
Davis TN, Sugiura M. 1966. Auroral electrojet activity index AE and its universal time variations. J Geophys Res. 71:785–801.
Eckman JP, Ruelle D. 1985. Ergodic theory of chaos and strange attractors. Rev Mod Phys. 57:617–628.
Elshorbagy A, Simonovic SP, Panu US. 2002. Estimation of missing stream flow data using principles of chaos theory. J Hydrol. 255:123–133.
Falayi EO, Adepitan JO, Oyebanjo OA. 2017. Geomagnetic field H, Z and electromagnetic induction features of coronal mass ejections in association with geomagnetic storm at African longitudes. Can J Phys. doi:10.1139/cjp-2017-0460
Falayi EO, Ogundile OO, Adepitan JO, Okusanya AA. 2018. Solar quiet variation of the horizontal and vertical components of geomagnetic field using wavelet analysis. Can J Phys. 2018–2034. doi:10.1139/cjp-
Fraser AM, Swinney HL. 1986. Independent coordinates for strange attractors from mutual information. Phys Rev. 33:1134–1140.
Fuwape IA, Ogunjo ST, Oluyamo SS, Rabiu AB. 2016. Spatial variation of deterministic chaos in mean daily temperature and rainfall over Nigeria. Theor Appl Climatol. doi:10.1007/s00704-016-1867-x
Ghamry E, Mahrous A, Fathy A, Salama N, Yumoto K. 2012. Signatures of the low-latitude Pi 2 pulsations in Egypt. NRIAG J Astron Geophys. 1:45–50.
Gkana A, Zachilas L. 2015. Sunspot numbers: data analysis, predictions and economic impacts. J Eng Sci Tech Rev. 8 (1):79–85.
Gwal AK, Rubeena S, Gopal P, Santosh JK. 2012. Study of seismic precursors by wavelet analysis. Res J Eng Sci. 1 (4):48–52.
Hafez AG, Ghamry E. 2011. Automatic detection of geomagnetic sudden commencements via time frequency clusters. Adv Space Res. 48(9):1537–1544.
Hafez AG, Khan TA, Kohda T. 2010. Clear Pwave arrival of weak events and automatic onset determination using wavelet filter banks. Digit Signal Process. 20(3):715–723.
Hajkowicz LA. 1998. Longitudinal (UT) effect in the onset of auroral disturbances over two solar cycles as deduced from the AE index. Ann Geophys. 16:1573–1579.
Han XH, Chang XM. 2013. An intelligent noise reduction method for chaotic signals based on genetic algorithms and lifting wavelet transforms. Inf Sci (Ny). 218:103–118.
Hanslmeier A, Brajša R. 2010. The chaotic solar cycle. Astronomy and Astrophysics. 509:A5.
Jani R, Ghorbani MA, Shamsai A. 2014. Dynamics of rainfall in Ramsar. J App 422 Sci Agri. 9(4):1371–1378.
Kennel MB, Brown R, Abarbanel HDI. 1992. Determining embedding dimension for phase space reconstruction using a geometrical construction. Phys Rev. 45:3403–3411.
Kumar P, Foufoula-Georgiou E. 1997. Wavelet analysis for geophysical applications. Rev Geophys. 35(4):285–412.
Liming HE, Lixin WU, Shanjun LIU, Baodong MA, 2011. Seismo-ionospheric anomalies detection based on integrated wavelet. Geoscience and Remote Sensing Symposium (IGARSS), Vancouver, British Columbia, Canada.
Mandrikova OV, Geppener VV, Goreva TS, Klionskiy DM, 2010. Multicomponent simulation and forecasting of a complex natural signal, International conference "Intelligent Information Processing" IIP-8, Cyprus, Paphos.
Mandrikova OV, Polozov YA, Bogdanov VV, Zhizhikina EA. 2012b. Method of detection of abnormal features in ionosphere critical frequency data on the basis of wavelet transformation and neural networks combination. J Software Eng App. 5(12B):181–187. doi:10.4236/jsea.2012.512b035.
Mandrikova OV, Polozov YA, Zaliaev TL, 2012a. Methods of analysis and interpretation of ionospheric critical frequency foF2 data based on wavelet transform and neural networks, European Seismological Commission 33rd General Assembly GA ESC 2012; [accessed 2012 Aug 19–24]. http://www.esc2012-moscow.org/files/GA_ESC_2012-Program_13.08.2012.xls.
Mandrikova OV, Solovjev IS, Geppener VV, Klionskiy DM. 2011. New wavelet-based approach intended for the analysis of subtle features of complex natural signals. Pattern Recognition and Image Analysis: New Information Technologies. 21(2):293–296.
Mandrikova OV, Solovjev IS, Geppener VV, Klionskiy DM. 2012c. Analyzing subtle features of natural time series by means of a wavelet-based approach. Pattern Recognit Image Anal. 22(2):323–332.
Mandrikova OV, Solovyev IS, Geppener VV, Klionskiy DM, Al-Kasasbeh RT. 2013. Analysis of the Earth's magnetic field variations on the basis of a wavelet-based approach. Digit Signal Process. 23:329–339.
Mayaud P. 1980. Derivation, meaning, and use of geomagnetic indicies. J Geophys Monogr. 22,:154.
NASA. Interface to produce plots, listings or output files from OMNI. http://omniweb.gsfc.nasa.gov/html/omni_min_data.html
Ogunsua BO, Laoye JA, Fuwape1 IA, Rabiu1 AB. 2014. The comparative study of chaoticity and dynamical complexity of the low-latitude ionosphere, over Nigeria, during quiet and disturbed days. Nonlin Process Geophys. 21:127–142.
Oludehinwa IA, Olusola OI, Bolaji OS, Odeyemi OO. 2014. Investigation of nonlinearity effect during storm time disturbance. Adv Space Res. 62:440–456.
Ossendrijver M. 2003. The solar dynamo. Astron Astrophys Rev. 11:287.
Rabiu AB, Ogunsua BO, Fuwape IA, Laoye JA. 2014. The comparative study of chaoticity and dynamical complexity of the low-latitude ionosphere, over Nigeria, during quiet and disturbed days. Nonlin Processes Geophys. 21:127–142.
Richardson IG, Cliver EW, and Cane HV. 2002. Long-term trends in interplanetary magnetic field strength and solar wind structure during the twentieth century. Journal of Geophysical Research. 107(A8):SSH–8
Rüdiger G, Hollerbach R 2004, The magnetic universe Weinheim: Wiley-VCH VCH. 95.
Sarp V, Kilcik,A. A, Yurchyshyn V, Rozelot JP, Ozguc A. 2018. Prediction of solar cycle 25: a non-linear approach. MNRAS. 481:2981–2985.

Sharma AS, Veeramani T. 2011. Extreme events and long-range correlations in space weather. Nonlin Proc Geophys. 18:719–725.

Shaw R. 1981. Strange attractors, chaotic behaviour, and information flow. Z Naturforsch. 36A:80.

Sivakumar B. 2000. Chaos theory in hydrology: important issues and interpretations. J Hydrol. 45:1–20.

Sivakumar B. 2004. Chaos theory in geophysics: past, present and future. Chaos, Solitons Fractals. 19 (2):441–462.

Suresh A, Selvaraj RS. 2017. Complete chaotic analysis on daily mean surface air temperature and humidity data of Chennai. J Ind Geophys Union. 21((4),):277–284.

Torrence C, Compo GP. 1998. A practical guide to wavelet analysis. Bull Amer Meteor Soc. 79(1):61–78.

Unnikrishnan K. 2008. Comparison of chaotic aspects of magnetosphere under various physical conditions using ae index time series, ann. Geophys. 26:941–953. doi: 10.5194/angeo-26-941-2008.

Unnikrishnan K. 2010. A comparative study on chaoticity of equatorial/low latitude ionosphere over Indian subcontinent during geomagnetically quiet and disturbed periods.. Nonlin Process Geophys. 17:765–776.

Unnikrishnan K, Ravindran S. 2010. A study on chaotic behaviour of equatorial/low latitude ionosphere over Indian subcontinent, using GPS-TEC time series. J Atmos Sol Terr Phy. 72:1080–1089.

Vasyliunas VM. 1975. Theoretical models of magnetic field line merging. Rev Geophys Space Phys. 13 (1):303–336.

Yang X-H, Meia Y, Shea D-X, Jian-Qiang L. 2011. Chaotic bayesian optimal prediction method and its application in hydrological time series. Comput Math with Appl. 61:1975–1978.

Zivkovic T, Rypdal K. 2011. Low-dimensionality and predictability of solar wind and global magnetosphere during magnetic storms. J Geophys Res. 116:a10215. doi:10.1029/2011ja016547